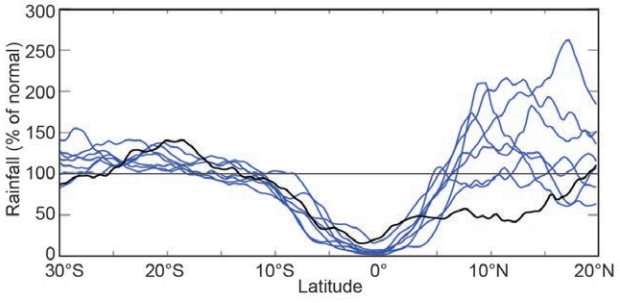

Fig. 4.30. South-north cross-sections of Jan–Mar rainfall anomalies (% of 1998–2011) for all La Niña seasons since 1998, averaged over the sector 180° to 150°W. The black line represents 2012, and the blue lines the years 1999, 2000, 2001, 2006, 2008, 2009, and 2011.

at Rarotonga (21°S, 160°W) in the southern Cook Islands it was 53% of normal (http://www.niwa.co.nz/climate/icu). These islands typically experience dry conditions during El Niño periods.

2) Atlantic—A. B. Pezza and C. A. S. Coelho

The Atlantic ITCZ is a well-organized convective band that oscillates approximately between 5°N and 12°N during July–November and 5°N and 5°S during January–May (Waliser and Gautier 1993; Nobre and Shukla 1996). Equatorial Kelvin waves can modulate the ITCZ intraseasonal variability (Wang and Fu 2007; Mounier et al. 2007; and Mekonnen et al. 2008); and ENSO is also known to influence it on the seasonal time scale (Münnich and Neelin 2005). In 2012 the prevailing equatorial Pacific scenario was a moderate La Niña that began retreating in March, leading to slightly warm to neutral conditions for the remaining of the year. The ITCZ responded to this pattern and presented a noticeable enhancement in January and February, with negative outgoing longwave radiation (OLR) anomalies in most of the western sector of the equatorial Atlantic surrounding South America (Fig. 4.31a). This pattern contributed to above-average rainfall in the Amazon sector of Brazil, Peru, Colombia, and Venezuela, but it was not sufficiently strong to produce significant rainfall in the drought-prone area of northeastern Brazil during the first three months of 2012 (Fig. 4.31b).

The ending of La Niña conditions in March helped enhance the ITCZ via Kelvin wave-induced upper level divergence in the western Atlantic sector during January and February. For the remainder of the year the ITCZ presented a near-normal convective intensity, with occasional bursts of severe convection towards the Caribbean Sea. This anomalous activity to the west responded to a cooler-than-average SST pattern in both the North and South Atlantic (Fig.

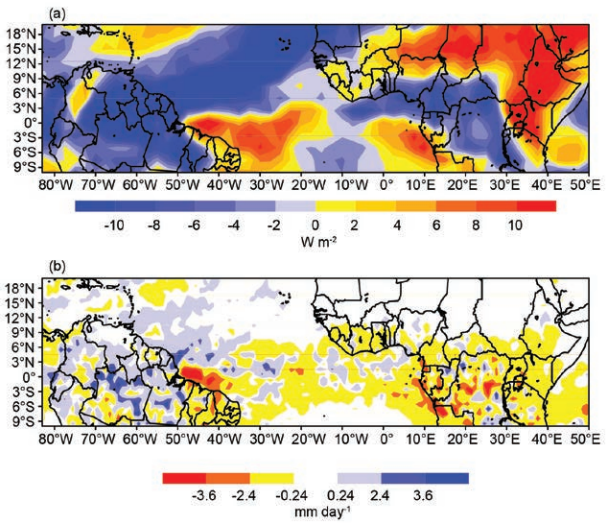

Fig. 4.31. (a) Atlantic NOAA interpolated OLR (Liebmann and Smith 1996) anomalies (W m^{-2}) for Jan–Feb 2012 and (b) TRMM anomalous precipitation rate (mm day^{-1}) for Jan–Mar 2012. Anomalies are based on the climatology for (a) 1975–2011 and (b) 1998–2011.

4.32a) prevailing until austral winter. Such an SST pattern favored the ITCZ predominant location to the north of its climatological position particularly during the first four months of the year. During boreal summer, the North Atlantic warmed up considerably and remained warm until the end of the year. The interplay of the SST gradient between the South and North Atlantic is seen by the Atlantic Index (see Fig. 4.32b caption for definition), which shows a return to negative conditions (unfavorable for convection within the ITCZ) contrasting with parts of 2010 and 2011, yet not as severe as in early 2010. Within this scenario, the ITCZ oscillated north of its average climatological position for most of the year, with precipitation well below average over most of northeastern Brazil (Fig. 4.33; see Sidebar 7.2 for more details on the drought in this region).

g. Atlantic warm pool—C. Wang

The Atlantic warm pool (AWP) is a large body of warm water in the lower latitudes of the North Atlantic, comprising the Gulf of Mexico, the Caribbean Sea, and the western tropical North Atlantic (Wang and Enfield 2001, 2003). Previous studies have shown that the AWP plays an important role in Atlantic tropical cyclone activity, and in rainfall in the central United States (Wang et al. 2006, 2008a, 2011). Unlike the Indo-Pacific warm pool, which straddles the equator, the AWP is entirely north of the equator. In addition to the large seasonal cycle, AWP variability occurs on both interannual and multidecadal timescales, and

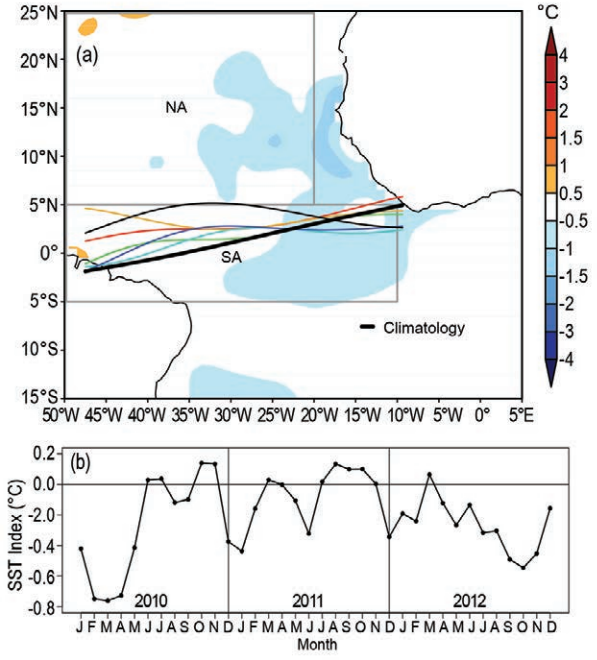

Fig. 4.32. (a) Atlantic ITCZ position inferred from OLR during Apr 2012. The colored thin lines indicate the approximate position for the six pentads of Apr 2012. The black thick line indicates the Atlantic ITCZ climatological position. The SST anomalies (°C; Reynolds et al. 2002) for Apr 2012 based on the 1982–2011 climatology are shaded. The two boxes indicate the areas used for the calculation of the Atlantic Index in (b). (b) Monthly SST anomaly time series averaged over the South American sector (SA region, 5°S–5°N, 10°W–50°W) minus the SST anomaly time series averaged over the tropical coast of northern Africa (NA region, 5°N–25°N, 20°W–50°W) for 2010–12 forming the Atlantic Index. The positive phase of the index indicates favorable conditions for enhanced Atlantic ITCZ activity.

has exhibited a long-term warming trend (Wang et al. 2006, 2008b). Figures 4.34a and b depict the long-term total and detrended June–November AWP area anomalies. The multidecadal variability (Fig. 4.34c) shows that the AWP was larger during the period 1930–60, as well as after the late 1990s; and smaller during the periods of 1905–25 and 1965–95. The periods for large and small AWPs coincide with the warm and cool phases of the AMO (Delworth and Mann 2000; Enfield et al. 2001). Wang et al. (2008b) showed that the influences of the AMO on tropical cyclone activity and climate might operate through the atmospheric changes induced by the AWP. The spatial distribution of AWP-related global SST anomalies is shown in Fig. 4.35, which depicts the AWP varied with the global SST on both interannual and multidecadal time scales.

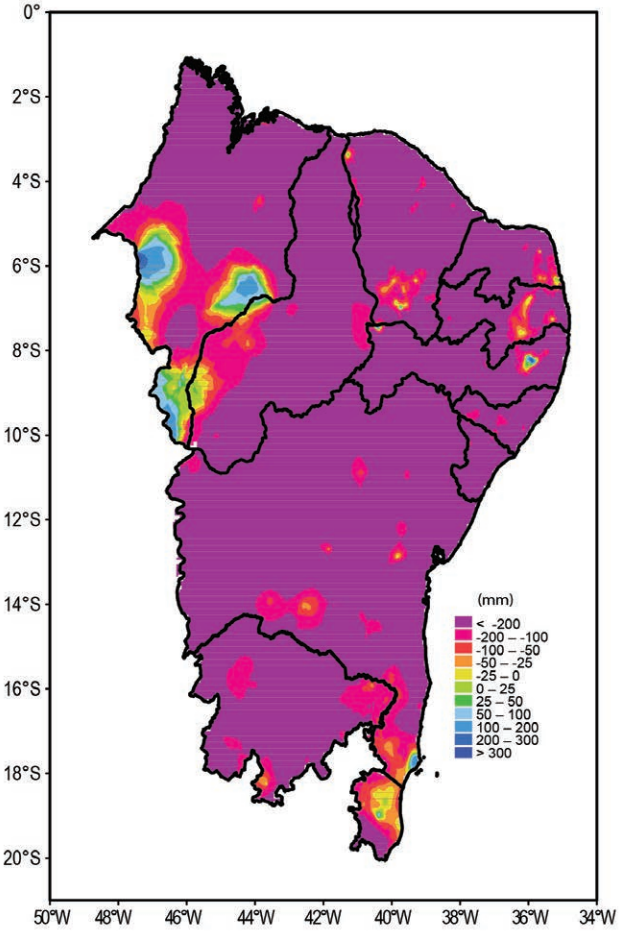

Fig. 4.33. Northeastern Brazil average 2012 precipitation anomaly (mm) with respect to 1961–90 climatology based on high resolution station data. [Data sources: federal and regional networks (CMCD/INPE, INMET, SUDENE, ANEEL, FUNCEME/CE, LMRS/PB, EMPARN/RN, LAMEPE/ITEP/PE, CMRH/SE, SEAAB/PI, SRH/BA, CEMIG/SIMGE/MG, SEAG/ES)].

In 2012, the AWP during the Atlantic hurricane season was larger than its climatological mean, with the largest AWP occurring in September (Fig. 4.36a). The large AWP in 2012 was associated with an active 2012 hurricane season in the North Atlantic, and consistent with that, a large AWP is generally associated with a reduction in vertical wind shear and an increase in atmospheric instability in the MDR—two factors favoring tropical cyclone development (Wang et al. 2008a). Spatially, the AWP started to develop in June in the Gulf of Mexico (Fig. 4.36b). By July and August, the AWP was well developed in the Gulf of Mexico and Caribbean Sea and reached eastward to the western tropical North Atlantic (Figs. 4.36c,d). By September, the AWP had further expanded southeastward and the isotherm of 28.5°C covered the entire tropical North Atlantic by crossing to the coast of

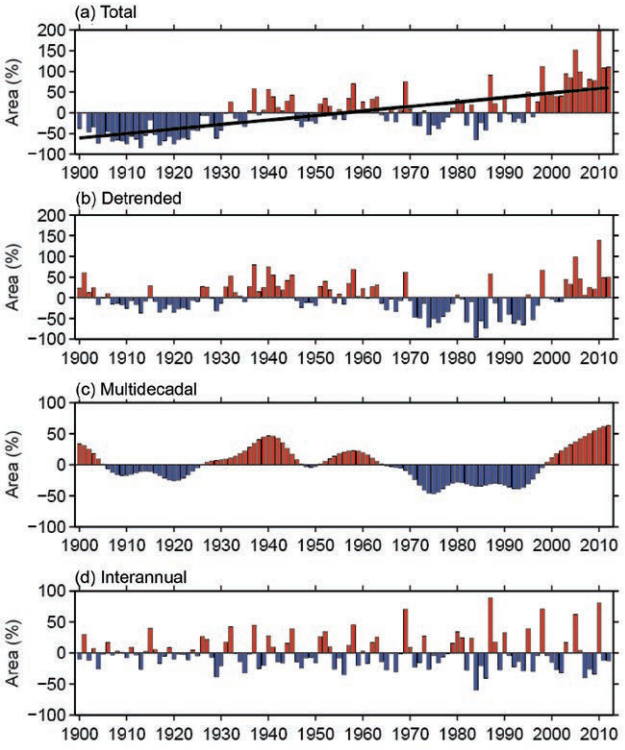

Fig. 4.34. The AWP index from 1900–2012. The AWP area index (%) is calculated as the anomalies of the area of SST warmer than 28.5°C divided by the climatological AWP area for Jun–Nov. Shown are the (a) total, (b) detrended (removing the linear trend), (c) multidecadal, and (d) interannual area anomalies. The multidecadal variability is obtained by performing a seven-year running mean to the detrended AWP index. The interannual variability is calculated by subtracting the multidecadal variability from the detrended AWP index. The black straight line in (a) is the linear trend that is fitted to the total area anomaly.

Africa (Fig. 4.36e). The AWP started to decay after October when the waters in the Gulf of Mexico began cooling (Figs. 4.36f,g).

Previous studies have shown that AWP variability also affects Atlantic hurricane tracks (Wang et al. 2011). An eastward expansion of the AWP tends to shift the focus of cyclogenesis eastward, thereby decreasing the possibility for hurricane landfall in the southeastern United States. A large AWP also weakens the North Atlantic subtropical high and produces the eastward tropical cyclone steering flow anomalies along the eastern seaboard of the United States. Due to these two mechanisms, hurricanes are generally steered toward the north and northeast. The 2012 hurricane season was consistent with this trend, as most storms formed in the eastern tropical North Atlantic and tended to move northward or northeastward.

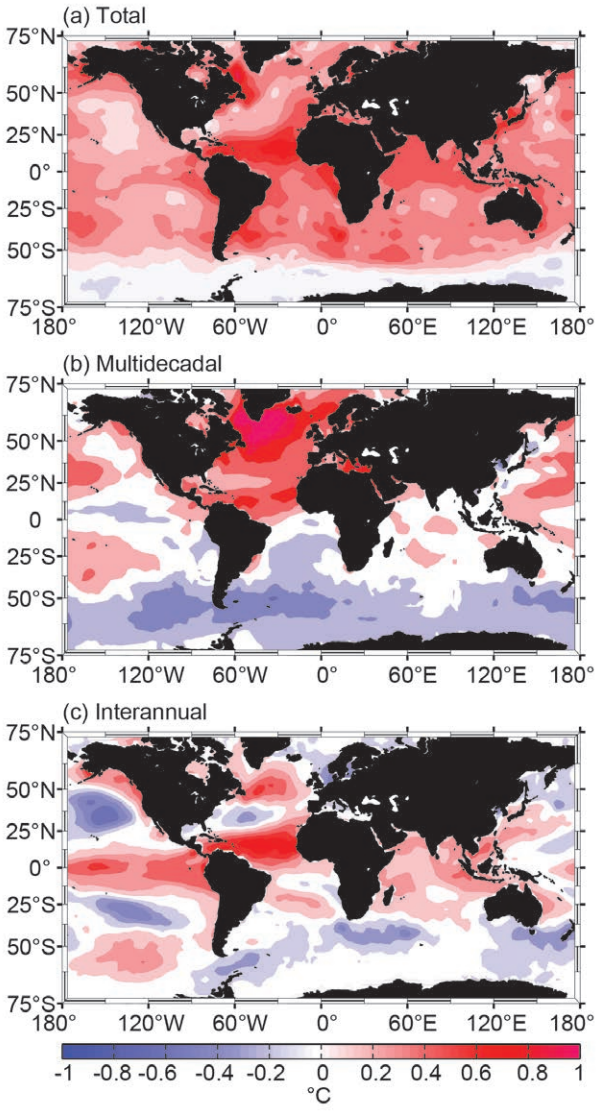

Fig. 4.35. Regression coefficients (°C per 100%) of the global SST anomalies during Jun–Nov onto the AWP (a) total, (b) multidecadal, and (c) interannual area indices in Fig. 4.34. The SST anomalies are calculated as departures from the 1971–2000 climatology.

h. Indian Ocean dipole—J.-J. Luo

The Indian Ocean dipole (IOD)—a climate mode in the tropical Indian Ocean—usually starts in boreal summer, peaks in Northern Hemisphere fall, and decays rapidly in early boreal winter. The IOD is a major air-sea coupled climate mode in the tropical Indian Ocean, which often brings about considerable environmental and socioeconomic impacts to countries surrounding the Indian Ocean. During the boreal summer and fall of 2012, a positive IOD event (with anomalous SST cooling in the eastern Indian Ocean and warming in the west) occurred.

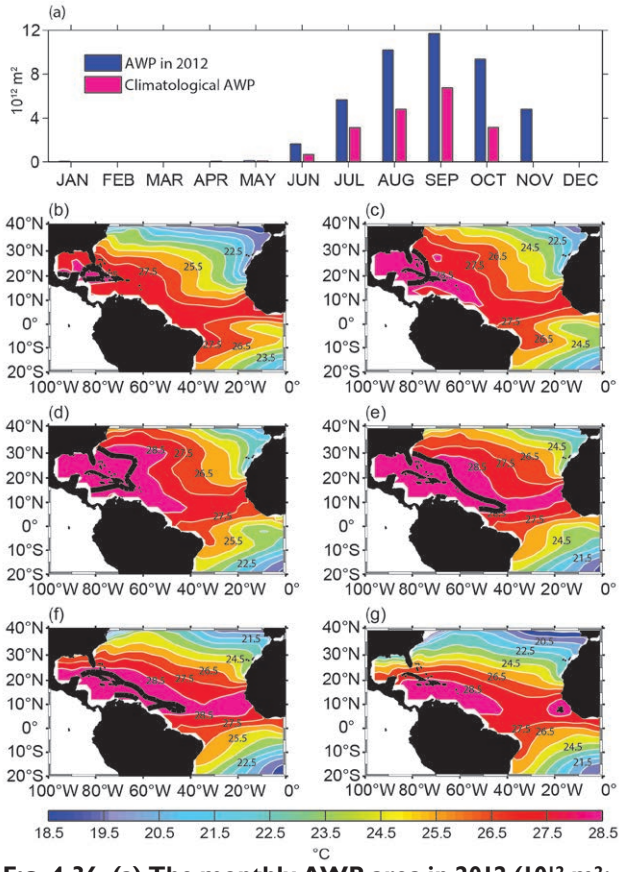

Fig. 4.36. (a) The monthly AWP area in 2012 (10^{12} m^2; blue) and the climatological AWP area (red). Spatial distributions of the 2012 AWP in (b) Jun, (c) Jul, (d) Aug, (e) Sep, (f) Oct, and (g) Nov. The AWP is defined by SST larger than 28.5°C. The black contours in (b–g) are the climatological AWP normals based on 1971–2000.

This Indian Ocean dipole was short-lived: it began in July and dissipated in November. Its peak intensity in August was greater than two standard deviations and became the fourth strongest event over the past three decades (Fig. 4.37b). However, unlike the three extreme events in 1994, 1997, and 2006, which were predominantly determined by strong cooling in the eastern IO, the warming in the western Indian Ocean contributed more than the cooling in the east to the 2012 IOD (Fig. 4.37a). This may be related to the fact that the mean tropical Indian Ocean Basin SST has risen rapidly in recent decades, two to three times faster than that of the Pacific (Luo et al. 2012). The east cooling-west warming SST dipole structure is well-linked with stronger-than-normal surface easterlies in the central equatorial IO (Fig. 4.37b); this is a typical air-sea coupled feature of the IOD. In contrast to the positive IOD in 2011, which occurred with a La Niña, the 2012 positive IOD occurred with a weak El Niño-like condition.

Associated with the 2011/12 La Niña, anomalous easterlies in the western-central Pacific and westerlies in the Indian Ocean converged in the Indonesia area. This produced stronger-than-normal rainfall in the eastern Indian-western Pacific during late 2011 and into early 2012 (Figs. 4.38a,b). The La Niña also caused wet conditions in southeastern Australia. Meanwhile, warm water piled up in the western Pacific, due to the Pacific easterly anomalies, and penetrated into the IO via the Indonesian throughflow. The warm water propagated southward along the west coast of Australia via coastal Kelvin waves and extended westward via Rossby waves (Fig. 4.39). The oceanic downwelling Rossby waves induced basinwide SST warming in the South Indian Ocean with a shape being oriented in the southeast-northwest direction (Fig. 4.38). The SST warming promoted strong-than-normal rainfall and local surface wind convergence. As a result of the atmospheric Rossby wave response to the SST warming, a cyclonic wind anomaly formed with its center always shifted poleward of the SST warming.

Following the 2011/12 La Niña, weak El Niño conditions developed in the second half of 2012. Equatorial SST warming showed a westward propagation consistent with this El Niño condition.

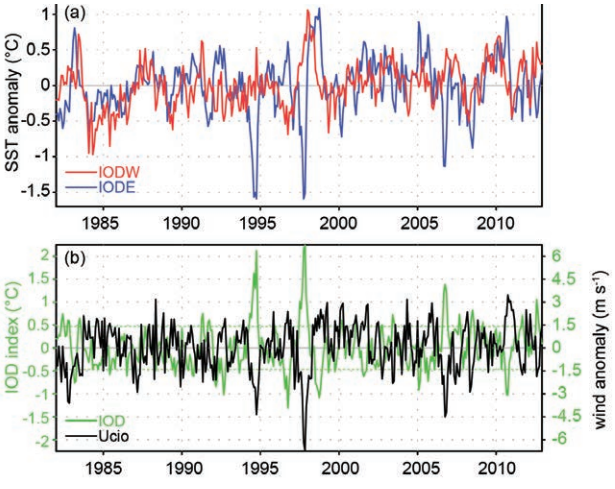

Fig. 4.37. (a) Monthly anomalies of SST (°C) in the eastern (IODE; 90°E–110°E, 10°S–0°, blue lines) and western poles (IODW; 50°E–70°E, 10°S–10°N, red lines) of IOD. (b) As in (a), but for the IOD index (°C; measured by the SST difference between IODW and IODE, green line) and surface zonal wind anomaly (m s^{-1}) in the central equatorial IO (Ucio), from 70°E–90°E, 5°S–5°N (black line). The anomalies were calculated relative to the 1982–2011 climatology; based on the NCEP optimum interpolation SST (Reynolds et al. 2002) and JRA-25 atmospheric reanalysis (Onogi et al. 2007).